Desalination and Water Treatment
www.deswater.com
doi: 10.5004/dwt.2023.29377

289 (2023) 111–122
March

3D-printed amidoximed hollow spheres with enhanced selectivity and antifouling property for uranium recovery from wastewater

Jinmei Li[a], Pin Gao[a], Nan Li[a,b], Zhining Wang[a,*]

[a]*Shandong Provincial Key Laboratory of Water Pollution Control and Resource Reuse, School of Environmental Science and Engineering, Shandong University, Qingdao 266237, China, Tel.: +86-0532-58630929; emails: wangzhn@sdu.edu.cn (Z. Wang), 1037055614@qq.com (J. Li), gaopin616@163.com (P. Gao), linanhhh@sdu.edu.cn (N. Li)*
[b]*School of Information Science and Engineering, Shandong University, Qingdao 266237, China*

Received 17 November 2022; Accepted 20 February 2023

ABSTRACT

Natural seawater is a kind of sustainable source to provide uranium in the future. Uranium extraction from seawater faces great challenges, including weak mechanical strength, poor selectivity and severe fouling. In this paper, based on the principle of additive manufacturing technology, poly(amidoxime)-loaded hollow spheres (3D-PAO) with multilayer skeleton structures were prepared via 3D printing method. The adsorption process matched the Langmuir isotherm model better and the calculated maximum U(VI) uptake on 3D-PAO was 78.01 mg/g. In addition, 3D-PAO presented high selectivity to U(VI) against other coexisted metal ions. In addition, the regeneration efficiency of 3D-PAO reached a high value of 71.63% after six-time regeneration, and 3D-PAO still displayed great reusability with the coexistence of different oils. This work provided a feasible strategy to improve the selectivity, mechanical strength and antifouling performance of uranium adsorbents and opens a new avenue for oceanic uranium extraction.

Keywords: Uranium; Adsorption; Amidoxime group; 3D printing; Hollow spheres

1. Introduction

The sustainable supply of energy is the cornerstone of human progress and development [1,2]. Given that the increasing energy demands and deteriorated environmental problems during the use of fossil fuels, nuclear power has been considered as a potential alternative [3,4]. Uranium, as a prime fuel applied in nuclear reaction, has been widely distributed in terrestrial ores and ocean [5]. However, the uranium containing wastewater discharged from uranium mining and nuclear testing could inflict hazardous damage on groundwater and ecological systems owing to their radioactivity and chemical toxicity. The World Health Organization requires that the maximum uranium concentration should not be higher than 14 μg/L in drinking water [6], the uranium concentration in uranium mining wastewater cannot exceed 5 mg/L [7]. Therefore, the elimination of uranium from wastewater is of great urgency [8].

Many methods have been studied and applied extensively for the treatment of uranium, such as adsorption [9,10], membrane processing [11], precipitation [12] and electrodeposition [13]. Owing to the advantages of the low cost and easy operation, adsorption has been considered as one of the most promising methods to extract uranium. Adsorbents with high specific surface area, such as metal–organic frameworks [14], silica aerogels [15], graphene aerogels [16], etc. However, coexisting ion competition, surface fouling and low strength of adsorbents worsen uranium capture arduousness [17]. Because of this, adsorbents with great selectivity, good mechanical strength and antifouling properties need to be developed.

* Corresponding author.

Adsorption ligand is an essential element that determines the behaviors of adsorbents. Effective ligands containing amidoxime [7], hydroxyl [15], carboxyl [18], phosphate [19], sulfonic acid [6] and amino groups [20] are usually used in selectivity improvement. Among the numerous ligands, amidoxime (AO) is the most popular since it manifests a strong binding force for uranyl ions [7]. Ahmad et al. [21] fabricated a flower-like porous polymer modified amidoxime, which could selectively trap uranium from simulated solution and seawater. Liu et al. [22] designed a highly efficient nanoclay-poly(amidoxime) hydrogel for uranium extraction, the hydrogel reached 8.62 mg/g uranium extraction from seawater in 25 d. However, the weak mechanical strength, complex synthesis process and recovery problems limit the practical application of the amidoximed adsorbents.

Three-dimensional (3D) printing is a sort of newly developed technique, which can build desired structures that have been impossible to construct priorly [23]. Compared with traditional processing methods, 3D printing can sharply reduce the processing time and manufacturing cost with a material utilization ratio of 100%. In addition, 3D-printed materials can exhibit excellent mechanical strength through controlling their shapes, structures and inks. Li et al. [24] used 3D printing to construct silica ceramic cores with enhanced mechanical properties, the ceramic flexural strengths were increased to a high level of 12.1 MPa. 3D-printed materials have also been used as potential adsorbents for uranium removal owing to the high geometric flexibility. Song et al. [25] fabricated a three-dimensional porous calcium alginate scaffold using 3D printing method for uranium removal, which possessed good stability for both microstructure and adsorption properties. 3D printing method can offer a low-cost and easily operated approach for solving weak mechanical strength, complex synthesis processes and recovery problems of amidoximed adsorbents.

Herein, we fabricated a hollow multilayer sphere modified by poly(amidoxime) (3D-PAO) via 3D printing as a new strategy for the application of PAO powder in U(VI) adsorption. The PAO powder was doped into the flowing resin and printed into the designed shape with a three-dimensional structure by a 3D printer. 3D-PAO composites amalgamate the advantages of both PAO and 3D print products with different structures, resulting in the further improvement of adsorption capacity, selectivity, mechanical strength and other properties in the resulting material. Specifically, the surface of multi-layer sphere was composed of triangles to improve the mechanical strength of 3D-PAO, which was also beneficial for uranyl transfer and improved uranium efficiency. The physico-chemical properties of 3D-PAO were determined by scanning electron microscopy (SEM), Fourier-transform infrared spectroscopy (FTIR), atomic-force microscopy (AFM), X-ray photoelectron spectroscopy (XPS) and contact angle test. Adsorption experiments were systematically performed to explore the performance and mechanisms of the adsorption. Furthermore, the selectivity, reusability and antifouling ability of the materials were systematically tested. Our work presented the rational design and synthesis of amidoxime-based adsorbents with outstanding performance for uranium extraction.

2. Materials and methods

2.1. Materials

Polyacrylonitrile (PAN) (M_w = 150,000) was got from Shanghai DiBo Co., Ltd., (Shanghai, China). Photopolymer resin was provided by FormLabs Co., Ltd, USA. Hydroxylamine hydrochloride ($NH_2OH{\cdot}HCl$), sodium hydroxide (NaOH), uranyl nitrate hexahydrate ($UO_2(NO_3)_2{\cdot}6H_2O$) and other reagents were provided by Shanghai Macklin Biochemical Co., Ltd., (Shanghai, China).

2.2. Synthesis of PAO

PAO was prepared from PAN powder through a facile method. First, PAN powder (3 g) and $NH_2OH{\cdot}HCl$ (4.5 g) were added to a three-necked flask filled with 21 mL methanol. Then, the mixture was reacted at room temperature with vigorous shaking to prevent the agglomeration of $NH_2OH{\cdot}HCl$ particles. Subsequently, 3.2 g NaOH was dispersed in 5 mL deionized water, the NaOH solution was poured into the above mixture. After keeping stirring at 70°C for 24 h with condensation reflux, warm deionized water was added to the mixture to form white precipitate. The white precipitate was washed by pure water and methanol, and then freeze dried to obtain PAO.

2.3. Preparation of 3D-PAO

The multi-layer hollow spheres were designed, each sphere is composed of three layers, and the radius of each layer is 2.7, 4.1 and 5.4 mm. The designed sphere model was transferred to the 3D printer terminal through the printer's software 'Preform', and the resin tank of 3D printer was filled with resin containing 20% PAO for printing. The product was washed to remove the excess resin on the surface of the material, followed by being dried at 35°C overnight to obtain the unstick multi-layer sphere containing PAO (3D-PAO). The multi-layer spheres without PAO (3D-original) were also printed in the same method. Other 3D-PAOs with different PAO ratios were also prepared and studied (Fig. S1).

2.4. Characterization

The porous structures were measured by N_2 adsorption/desorption experiments using a JW-BK122W surface area analyzer (Beijing JWGB). Dynamic light scattering (DLS, Malvern, Nano ZS90, UK) was applied to analyze the particle size. The surface morphologies of 3D materials were studied by SEM using a Hitachi S-4800 microscope (Japan). FTIR (Bruker, Tensor 27, German) and XPS (Thermo Fisher, Thermo ESCALAB 250Xi, USA) were used to determine the chemical structures and chemical elements on the surface of the 3D materials.

2.5. Adsorption/desorption tests

Adsorption tests with different adsorbents were carried out at 25°C in U(VI) solution (150 mL, 20 mg/L) by an oscillation box (IS-RDS6, Crystal, America) with a rotating speed of 150 rpm. The standard curve was shown Fig. S2 and the amount of U(VI) extracted by adsorbents was calculated by following expression:

$$q_e = \frac{(C_o - C_e)V}{m} \quad (1)$$

where q_e (mg/g) is U(VI) uptake on adsorbents; C_o and C_e (mg/L) are U(VI) concentrations at beginning and ending of adsorption; V (L) represents the solution volume and m (g) is the mass of PAO.

To elute the loaded uranium on the adsorbent, four eluants (0.1 mol/L HCl, 0.1 mol/L H_2O_2, 0.1 mol/L HCl + 0.1 mol/L NaOH, 0.1 mol/L H_2O_2 + 0.1 mol/L NaOH) were used. The 3D-PAO adsorbed U(VI) (3D-PAO/U) was soaked in 100 mL eluent for 60 min at 25°C, washed by pure water and dried at 45°C.

3. Results and discussion

3.1. Characterization of 3D-PAO

The surface morphologies of PAN, PAO, 3D-original and 3D-PAO were characterized by SEM (Fig. 1). Fig. 1a and b show that the PAN particles were evenly dispersed and displayed in the shape of pebbles. After amidoximation, the cobblestone shaped particles were damaged, the surface became angular and exhibited the shape of charred charcoal, and slight stacking were observed between particles (Fig. 1c). When the scanning electron microscope was magnified (Fig. 1b and d), the uniform pores were found on the surface of PAN particles, while the surface of the PAO powder presented in a granular morphology with long strip-shaped particle clusters. In Fig. 1e, the surface of 3D-original using the original transparent resin was relatively smooth with only transverse and longitudinal stripes, which was due to the inherent problems of laser printing in UV curing printers. In Fig. 1f, PAO particles were observed and evenly embedded on the resin surface, suggesting the successful synthesis of 3D-PAO.

The chemical structure of the material surface was determined by FTIR spectrum (Fig. 2). According to the FTIR spectrum of PAN (Fig. 2a), a characteristic peak at 2,245 cm^{-1} was caused by C≡N stretching. After amidoximation, the C≡N peak disappeared, three new characteristic peaks assigned to C=N, C–N and N–O were observed in 1,650; 1,386 and 941 cm^{-1}, respectively, which indicated that the nitrile group was successfully converted into amidoxime group under the action of hydroxylamine hydrochloride, proving the successful preparation of PAO. In addition, the FTIR spectra of 3D original and 3D-PAO were also measured (Fig. 2b). The characteristic peaks of the two overlapped more, but the peaks at 1,670; 1,392 and 960 cm^{-1} for 3D-PAO were strengthened due to the doping of PAO.

Fig. 3 displays the N_2 adsorption/desorption isotherms of 3D-original and 3D-PAO, which belonged to type III adsorption isotherms, indicating the mesoporous structures in the 3D materials [26]. The Brunauer–Emmett–Teller (BET) specific surface areas of 3D-original and 3D-PAO were 2.007 and 2.119 m^2/g, respectively, implying that the introduction of PAO could enlarge the BET specific surface area.

3.3. Effect of pH on U(VI) extraction

The solution pH value is one of the most vital factors for uranium adsorption, since pH could affect the form of U(VI) and the performance of adsorbent [27]. The effect of pH on U(VI) uptake was investigated with a single 3D-PAO

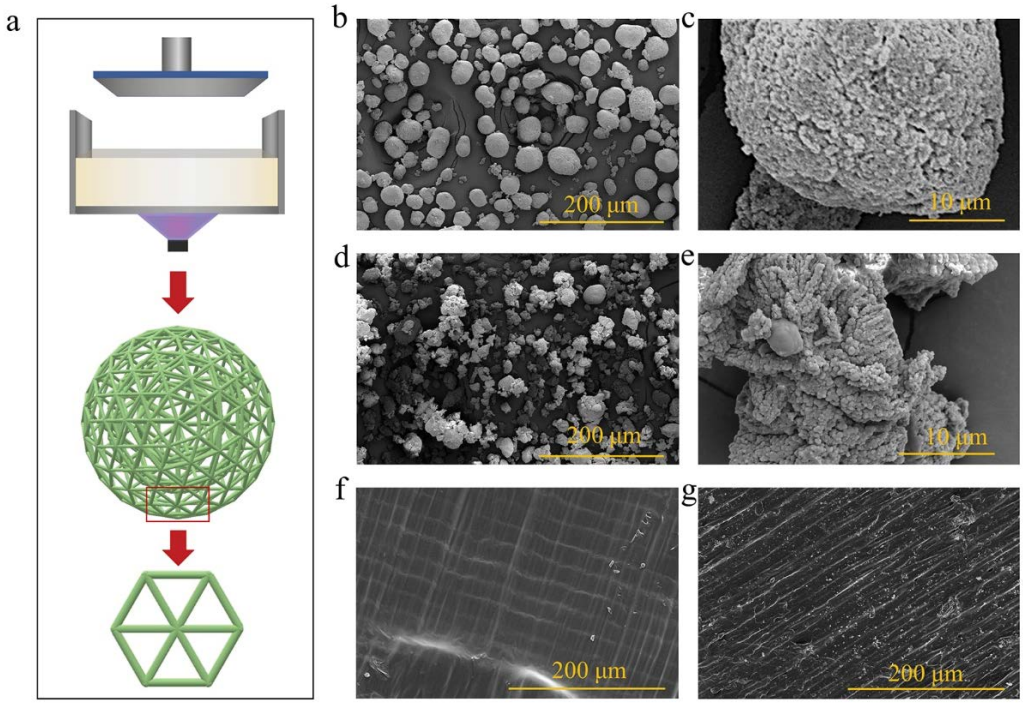

Fig. 1. (a) Scheme for the synthesis of 3D-PAO. Scanning electron microscopy images of (b, c) PAN, (d, e) poly(amidoxime), (f) 3D-original and (g) 3D-PAO.

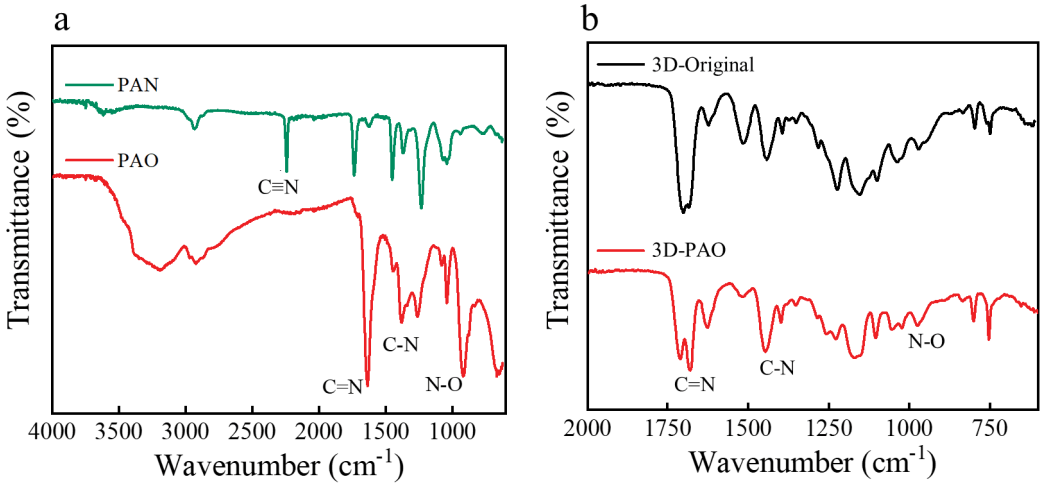

Fig. 2. Fourier-transform infrared spectra of PAN, poly(amidoxime), 3D-original and 3D-PAO.

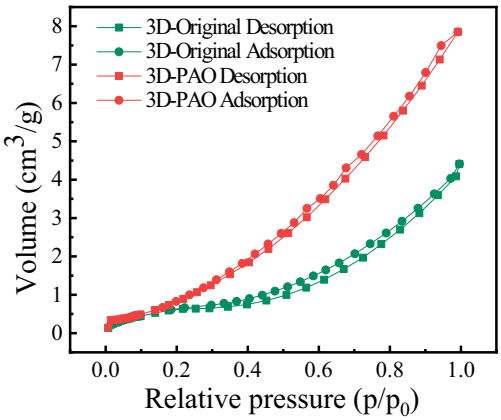

Fig. 3. N_2 adsorption/desorption isotherms of 3D-original and 3D-PAO.

sphere (0.22 ± 0.11 g) in uranium solution (150 mL, 20 mg/L) at pH range from 3.0 to 10.0 (Fig. 4 and Table S1). The adsorption capacity of 3D-PAO increased as the increase of pH, achieving the maximum (64.6 mg/g) when the pH value was 6.0. With the pH value of solution increased, the zeta potential of 3D-PAO became more negatively. At pH < 6.0, the main form of U(VI) is UO_2^{2+}, which was favorable for adsorption on more negatively charged 3D-PAO. While as the pH value further increasing, the U(VI) form converted to negatively charged anions, which caused strongly electrostatic repulsion between 3D-PAO and uranyl ions, resulting in the decrease of adsorption capacity.

3.4. Adsorption kinetics

The kinetics of the adsorption process were studied to describe the adsorption rate on 3D-PAO. In adsorption

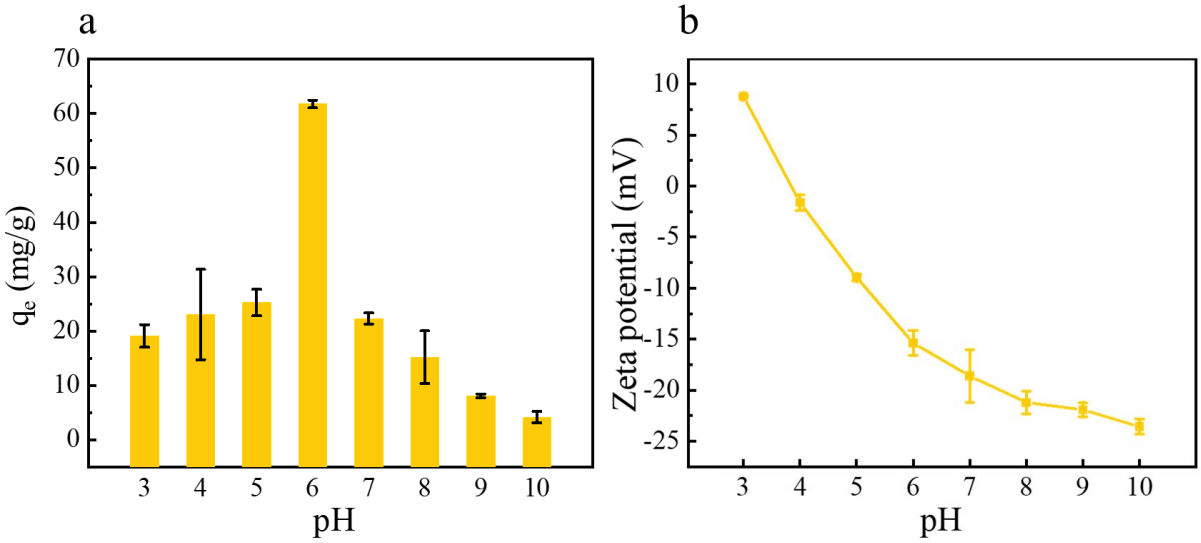

Fig. 4. (a) U(VI) uptake of 3D-PAO at varied pH values (m = 0.22 ± 0.11 g, V = 150 mL, C_o = 20 mg/L). (b) Zeta potential of 3D-PAO at varied pH values.

kinetics experiments, 150 mL of 20 mg/L U(VI) solution was used for adsorption at 25°C. The adsorption data at 5, 15, 30, 60, 120, 200, 340, 500, 700, 1,320 and 1,440 min were measured and fitted by following kinetic models:

Pseudo-first-order equation [28]:

$$\ln\left(q_e - q_t\right) = \ln q_e - k_1 t \tag{2}$$

Pseudo-second-order equation [29]:

$$\frac{t}{q_t} = \frac{t}{q_e} + \frac{1}{\left(k_2 q_e^2\right)} \tag{3}$$

where k_1 and k_2 represent the rate constants in two equations. q_e (mg/g) and q_t (mg/g) refer to the uptake of U(VI) at equilibrium and time t (min).

The fitting curve and kinetic parameters of two models were shown in Fig. 5 and Table 1, the adsorption process reached equilibrium within 1,500 min. According to the higher correlation coefficient (R^2 = 0.9951) of the pseudo-second-order kinetic adsorption model, the U(VI) adsorption on 3D-PAO is inferred as chemical adsorption.

3.5. Adsorption isotherms

The adsorption isotherm is a curve that describes changes of the adsorption amount in solutions with different concentrations under a certain temperature [5,30]. The adsorption performances of 3D-PAO were investigated by adsorption isotherms, 150 mL of U(VI) solutions with concentrations of 1, 5, 8, 10, 15, 20 and 30 were used. The adsorption was performed at 25°C for 1,500 min at 120 rpm. The experimental data were fitted by three models.

Langmuir isotherm [31]:

$$q_e = \frac{K_L q_{\max} C_e}{\left(1 + K_L C_e\right)} \tag{4}$$

Freundlich isotherm [32]:

$$q_e = K_f C_e^{1/n} \tag{5}$$

Temkin isotherm [33]:

$$q_e = a + b \log C_e \tag{6}$$

where $q_{\max}$ represents the maximum amount of U(VI) absorbed on 3D-PAO. The constants K_f and $1/n$ in Freundlich model denote the adsorption capacity and intensity. The constants, a and b in Temkin model, are obtained via the intercept and slope of the regression line.

U(VI) adsorption isotherms for U(VI) adsorption by 3D-PAO and fitted parameters are shown in Fig. 6a–c and Table S2. The highest degree of correlation was obtained by Langmuir adsorption isotherm with R^2 = 0.986 against Freundlich and Temkin adsorption isotherms (0.969 and 0.851), signifying that monolayer chemical adsorption dominated the adsorption process. The maximum adsorption capacity calculated was 78.01 mg/g, which is much higher than the related 3D-printed adsorbents (Table S3).

Table 1
Kinetic parameters of two models

Pseudo-first-order		Pseudo-second-order	
k_1 (min^{-1})	1.61×10^{-3}	k_2 (g/mg·min)	7.44×10^{-5}
q_e	64.02	q_e	68.72
R^2	0.9935	R^2	0.9951

3.6. Regeneration of 3D-PAO

Reusability is one of the important indexes that influence the application of adsorbents [34]. Four eluents were selected to regenerate 3D-PAO adsorbed U(VI) (3D-PAO/U). 3D-PAO/U was placed in 100 mL eluent and oscillated at 25°C with the speed of 120 rpm for 30 min, then the material was taken out washed with reverse osmosis water for many times until the pH of supernatant remained unchanged.

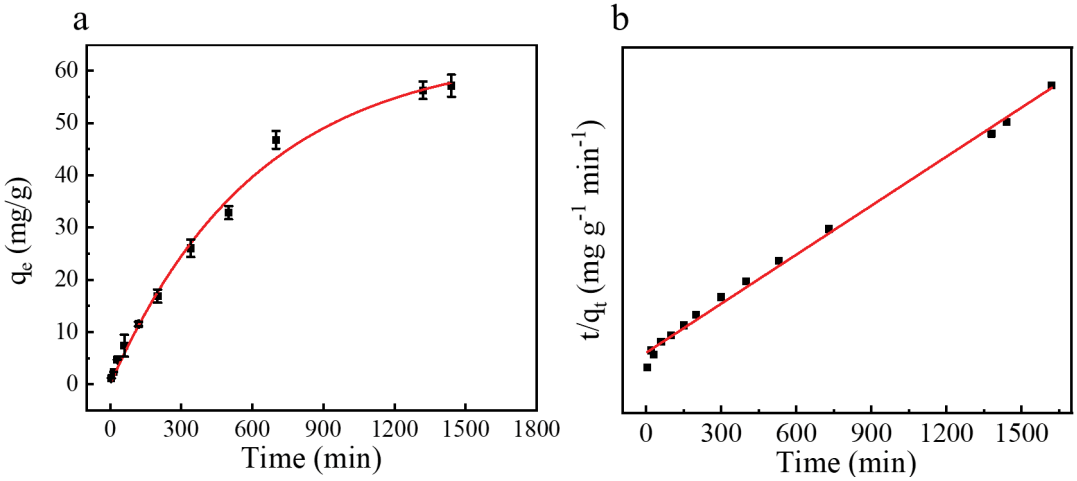

Fig. 5. (a) Pseudo-first-order and (b) pseudo-second-order kinetics models for U(VI) adsorption by 3D-PAO.

The eluted material was dried at room temperature, and then the adsorption experiment and elution experiment were repeated. The recycling efficiency (RE) was evaluated by the equation as follows:

$$\mathrm{RE} = \frac{Q_N}{Q_1} \times 100\% \quad (7)$$

where Q_1 (mg/g) is the extraction uptake in the first adsorption experiment. Q_N (mg/g) is the extraction amount obtained from the regeneration experiment, N refers to adsorption times.

Fig. 7a shows the U(VI) extraction capacity of 3D-PAO using different eluents during the regeneration experiments. With the increase of the adsorption/desorption recycle number, the U(VI) amount of 3D-PAO gradually decreased. The eluent containing 0.1 mol/L H_2O_2 and 0.1 mol/L NaOH exhibited the best performance for regeneration. After five cycles of adsorption/desorption using H_2O_2 and NaOH mixture, the recycling efficiency reached 97.26%, 97.36%, 94.92%, 75.78% and 71.63%, respectively, which implying the good reusability and stability of 3D-PAO.

3.7. Selectivity of 3D-PAO

Selectivity of adsorbents determine the adsorption performance and life span in real water samples [35]. To explore the selectivity of 3D-PAO, Na^+, Fe^{3+}, Cu^{2+}, Ca^{2+}, Mg^{2+}, K^+, Ba^{2+}, Sr^{2+} were selected as interfering ions. The concentrations of various metal ions before and after adsorption were detected via inductively coupled plasma mass spectrometry. As seen from Fig. 8, the adsorption capacity of 3D-PAO

Table 2
Value of underwater oil contact angle of material (pump oil, mineral oil, silicone oil and 1,2-dichloroethane

Oil	Contact angle (°)	
	1/70	70/70
Pump oil	131.3	131.2
Mineral oil	127.8	125.0
Dimethyl silicone oil	133.3	130.8
1,2-dichloroethane	123.1	93.2
DI water	43.9	32.0

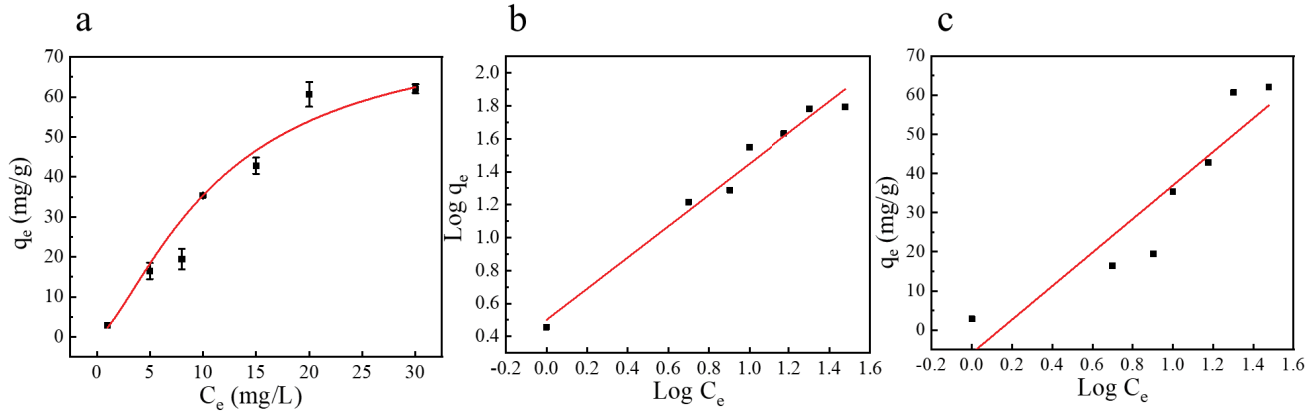

Fig. 6. (a) Langmuir, (b) Freundlich and (c) Temkin fitted plots for U(VI) extraction by 3D-PAO.

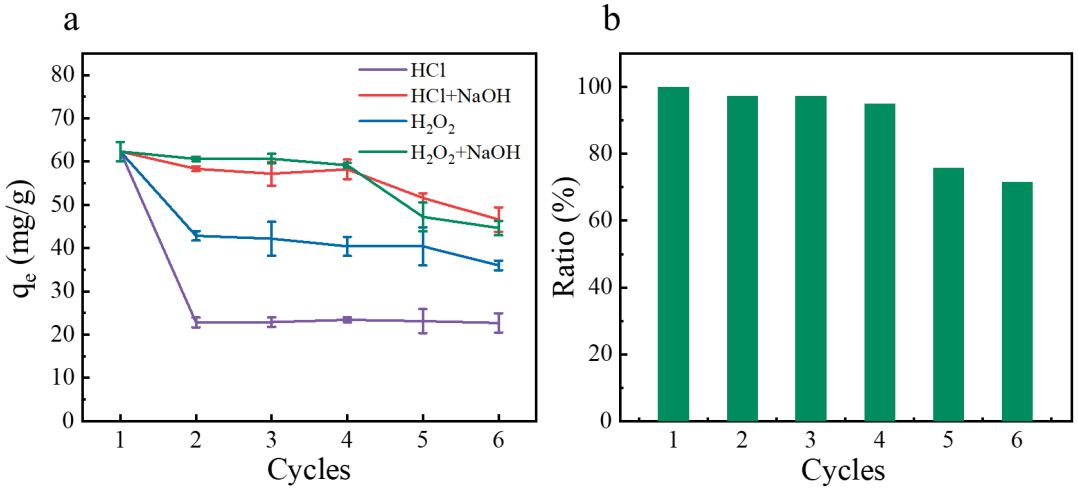

Fig. 7. (a) Adsorption capacity of 3D-PAO for U(VI) using different eluents and (b) the recycling efficiency of 3D-PAO.

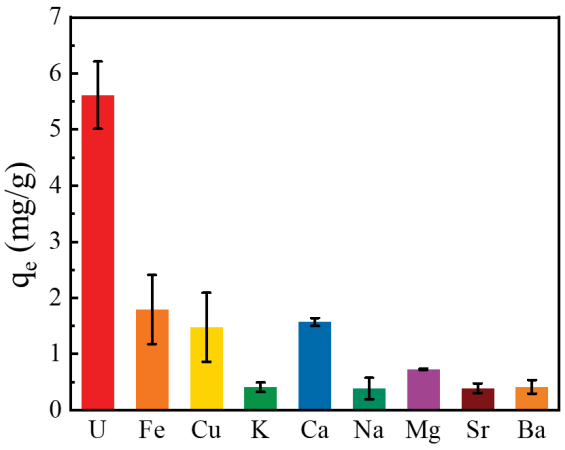

Fig. 8. Extraction uptake of 3D-PAO for different metal ions.

for U(VI) is the highest, showing that 3D-PAO has a good selectivity for U(VI). Amidoxime group contains amino nitrogen and oxime oxygen, which can donate electron and chelate uranyl ions. In addition, the amphoteric properties endow the amidoxime group strong binding force with UO_2^{2+} [11,36], resulting in the great reusability of 3D-PAO.

3.8. Adsorption mechanisms

FTIR and XPS spectra were used to study the adsorption mechanisms of 3D-PAO (Fig. 9). In Fig. 9a, the FTIR infrared spectra of 3D-PAO and 3D-PAO/U were compared, and a new peak appeared at 923 cm^{-1} after adsorption, which was caused by the antisymmetric tensile vibration of O=U=O [37]. The effective adsorption was also verified by EDC mapping in Figs. S3 & S4 and Table S4. The characteristic peaks of U 4f at around 392.10 and 381.05 eV were also observed via XPS spectra of 3D-PAO/U (Fig. 9b), the

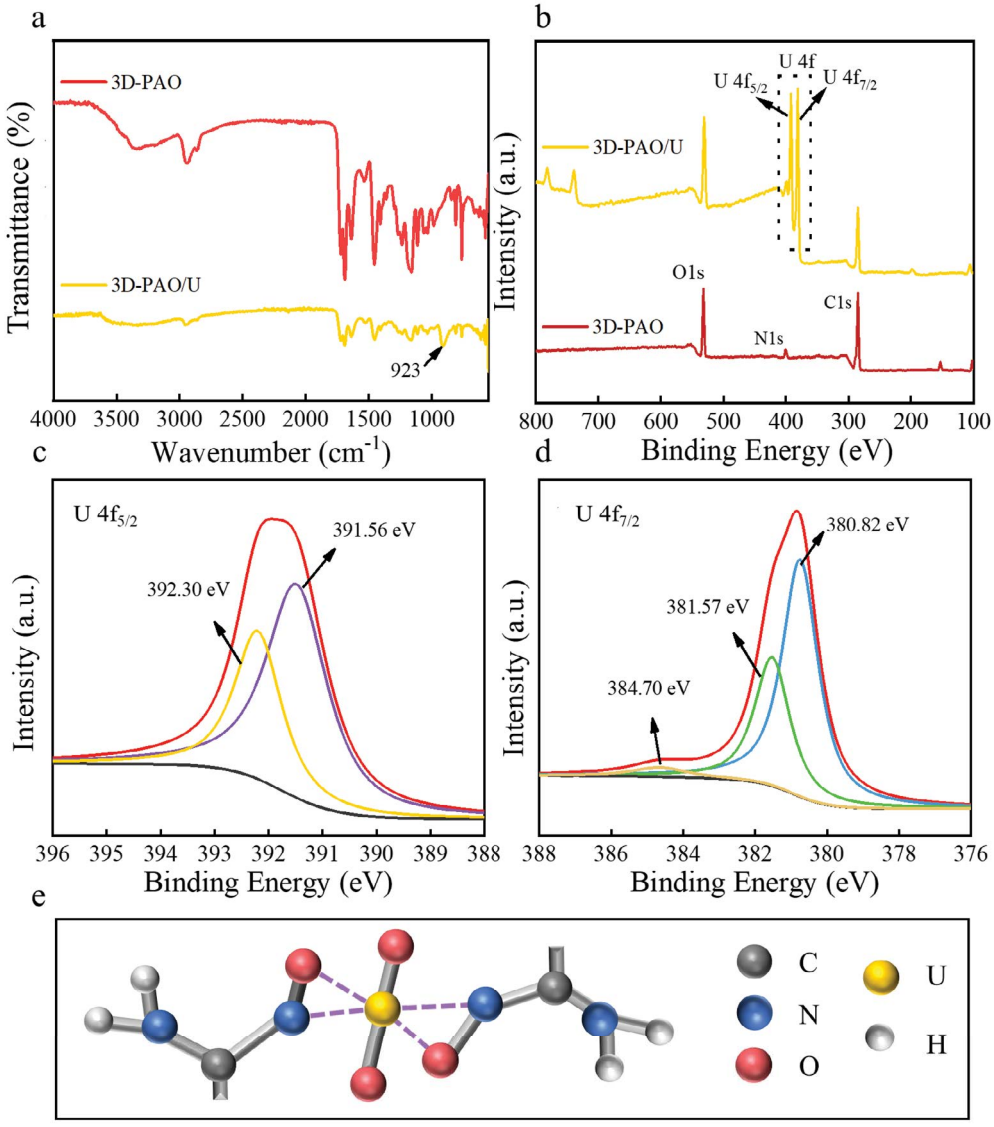

Fig. 9. (a) Fourier-transform infrared spectroscopy and (b) X-ray photoelectron spectroscopy of 3D-PAO and 3D-PAO/U. High-resolution of (c) U $4f_{5/2}$ and (d) U $4f_{7/2}$ of 3D-PAO/U. (e) Possible coordination between 3D-PAO and uranyl ions.

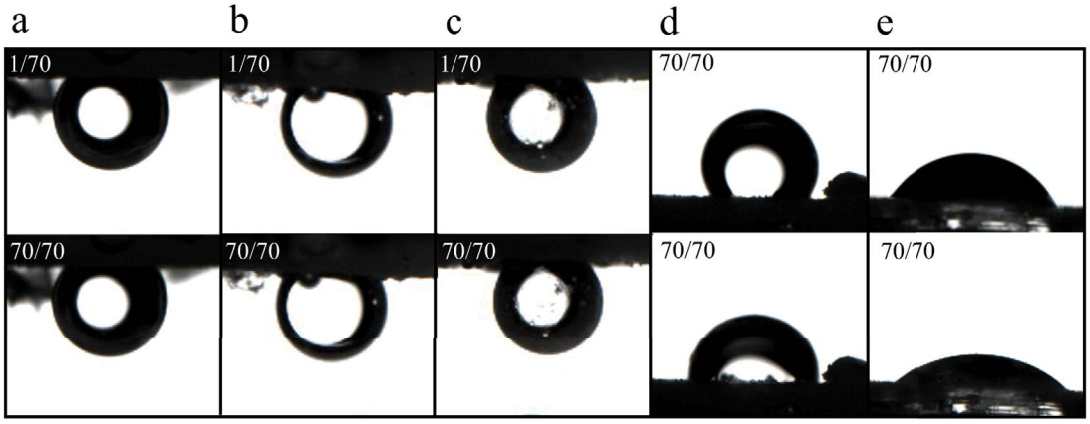

Fig. 10. The photos of underwater oil contact angle with (a) pump oil, (b) mineral oil, (c) silicone oil, (d) 1,2-dichloroethane of 3D-PAO, and (e) the water contact angle of 3D-PAO.

two peaks were assigned to U $4f_{5/2}$ and U $4f_{7/2}$, respectively [38,39]. The N base displayed a certain degree of red shift owing to the U(VI) adsorption, implying that interacted with $–NH_2$/–NH– via the lone electrons of carbon atom to nitrogen or oxygen in PAO [10]. It can be proved that U(VI) in the solution has been adsorbed to the adsorbent surface [40]. The two characteristic peaks of U 4f were further analyzed, and the U 4f was divided into U $4f_{5/2}$ and U $4f_{7/2}$ at 391.56, 392.30, 381.57 and 384.70 eV (Fig. 9c–d), which was caused by different valence states of U [41]. The coordination between 3D-PAO and uranyl ions was exhibited in Fig. 9e, uranyl ions were adsorbed onto amidoxime groups in 3D-PAO and formed η^2-type complexes, and (N, O) 2p on the oxime moiety has a strong covalent interaction and orbital hybridization with U 5f/6d [42].

3.9. Oil resistance of 3D-PAO

Hydrophilic and oleophobic properties are significant indicators to evaluate the oil resistance of adsorbents. The oil resistance of 3D-PAO can be preliminarily estimated by measuring the water contact angle and underwater oil contact angle. Three kinds of light oil and one kind of heavy oil were selected to test. Light oils were pump oil, mineral oil, dimethyl silicone oil and the heavy oil was 1,2-dichloroethane. The contact performance was recorded at the speed of intercepting 70 photos every 5 s. The first photo and the 70th photo were chosen to measure the contact angle of 3D-PAO and the specific values were shown in Table 2. In Fig. 10a–c, when light oils contacted the surface of 3D-PAO, all underwater oil contact angles were larger than 90°, and the contact angles nearly unchanged after 5 s. When the heavy oil contacted 3D-PAO for 5 s, the contact angle decreased slightly, but it still kept the oil drainage state (Fig. 10d). In addition, Fig. 10e shows the water contact angle of 3D-PAO, when the water droplets contacted 3D-PAO surface, they immediately dispersed, and the contact angle decreased from 43.9° to 32° after 5 s. This may be attributed to the hydrophilicity and hydrophobicity of amino and hydroxyl groups in 3D-PAO.

To investigate the effect of oil pollution on uranium extraction, pump oil, mineral oil, silicone oil and 1,2-dichloroethane were homogeneously mixed in 20 mg/L U(VI) solution at a volume ratio of 0.1%, respectively. Adsorption experiments in the mixture were performed at 150 rpm. After 24 h, the concentration of U(VI) in the mixed solution was detected and compared with the adsorption results in pure U(VI) solution. As shown in Fig. 11, the U(VI) extraction uptake on 3D-PAO coexisted with pump oil, mineral oil, silicone oil and 1,2-dichloroethane was 79.69%, 81.06%, 79.55% and 81.74% of that of pure U(VI) solution, implying the good oil pollution resistance of 3D-PAO.

At the same time, the regeneration experiments of 3D-PAO were also carried out in the oil-resistant experiment to determine the effect of oils on regeneration. The mixture of 0.1 mol/L H_2O_2 and 0.1 mol/L NaOH was used as the eluent, after desorption at 120 rpm at 25°C for 30 min, the 3D-PAO spheres were cleared for 5 min with assistance of ultrasound. Fig. 11b shows the U(VI) uptake on 3D-PAO after five cycles in pure U(VI) solution with/without oils coexisted. The trend of adsorption capacity of 3D-PAO in U(VI)-oil mixture was basically the same as that in pure U(VI) solution, while the U(VI) uptake decreased slightly, which was caused by the interference of oil on desorption. The photos of 3D-PAO spheres after five adsorption elution tests are shown in Fig. 11c, the color of all the spheres became shallow, indicating the effective desorption with the coexistence of oil pollution. This may be due to the hydrophilicity and hydrophobicity of 3D-PAO. Therefore, it can be considered that 3D-PAO has a good performance in the anti-oil pollution.

4. Conclusions

In summary, a kind of 3D-PAO hollow sphere was designed and constructed via 3D printing for uranium removal and extraction. The spherical multilayer skeleton made it convenient for adsorbent recycling and reuse. The adsorption isotherm fitted Langmuir adsorption model better, and the theoretical maximum extraction capacity was 78.01 mg/g. After 6 adsorption/desorption cycle experiments, the reusability of 3D-PAO reached 71.64%. In uranium solution with oil pollution, 3D-PAO still exhibited good reusability. In addition, 3D-PAO displayed good

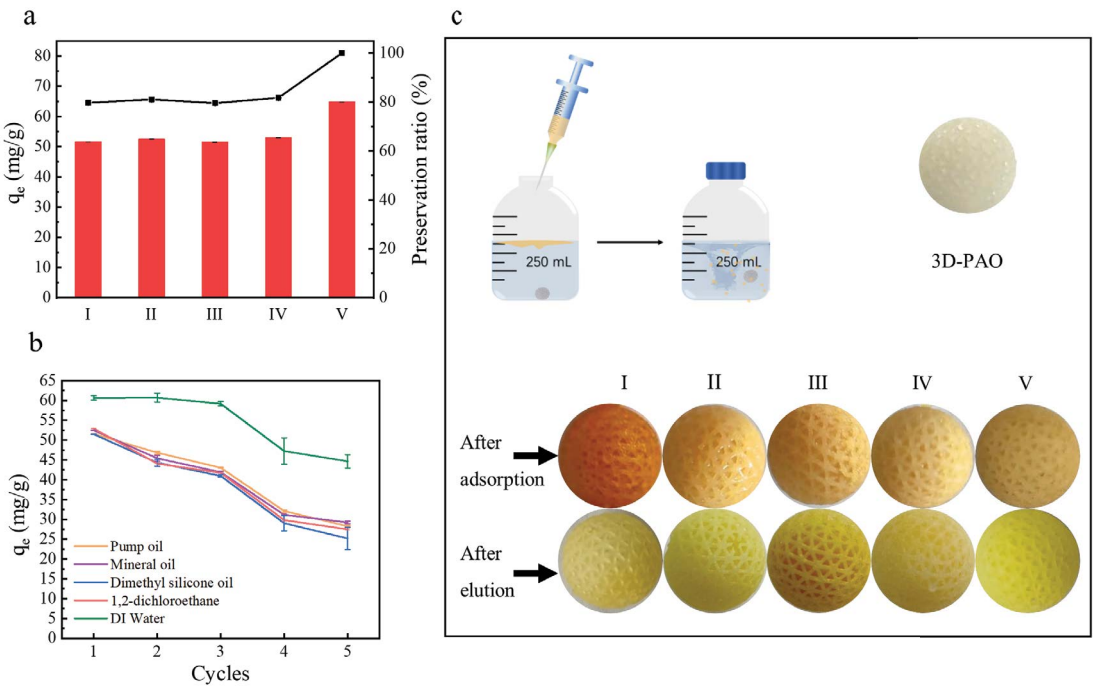

Fig. 11. (a) Effect of pump oil (I), mineral oil (II), dimethyl silicone oil (III), 1,2-dichloroethane (IV) and deionized water (V) on adsorption of 3D-PAO. (b) Effect of oil pollution on the adsorption of 3D-PAO during five adsorption–desorption. (c) Photos of 3D-PAO before adsorption, after adsorption and after elution.

selective adsorption for U(VI) against other competing ions due to the strong binding force between amidoxime and UO_2^{2+}. This work offers a novel method for constructing adsorbents with various shapes, good selectivity and great oil-resistant ability, which demonstrates great potential for ocean uranium extraction.

CRediT authorship contribution statement

Jinmei Li: Conceptualization, Methodology, Formal analysis, Investigation, Data Curation, Writing – Original Draft. Pin Gao: Conceptualization, Methodology, Formal analysis, Investigation, Data Curation, Writing – Original Draft. Nan Li: Writing – Review & Editing, Funding acquisition. Zhining Wang: Conceptualization, Funding acquisition, Project administration, Supervision, Writing – Review & Editing.

Declaration of competing interest

The authors declare that they have no known competing financial interests or personal relationships that could have appeared to influence the work reported in this paper.

Data availability

The data that has been used is confidential.

Acknowledgements

This work was financially supported by the National Natural Science Foundation of China (22078175 and 22208193), China Postdoctoral Science Foundation (2022M721927), Technological Innovation Projects of Shandong Province (2022CXGC021002), the Natural Science Foundation of Shandong Province (ZR2021LFG010 and ZR2022QB213), Postdoctoral Innovation Project of Shandong Province (SDCX-ZG-202202012).

Symbols

a	—	Constant in Temkin model, –
b	—	Constant in Temkin model, –
C_o	—	Initial U(VI) concentration, mg/L
C_e	—	Equilibrium U(VI) concentration, mg/L
k_1	—	Rate constant of pseudo-first-order equations, min^{-1}
k_2	—	Rate constant of pseudo-second-order equations, g/(mg·min)
K_f	—	Constant in Freundlich model, –
m	—	Mass, g
$1/n$	—	Constant in Freundlich model, –
Q_1	—	Adsorption amount in the first adsorption experiment, mg/g
Q_N	—	Adsorption amount obtained from the regeneration experiment, mg/g, N refers to adsorption times, –
q_e	—	Uptake of U(VI) at equilibrium, mg/g
q_{max}	—	Maximum amount of U(VI) absorbed, mg/g
q_t	—	Uptake of U(VI) at time t, mg/g
R	—	correlation coefficient, –
RE	—	Recycling efficiency, %
t	—	Time, min
V	—	Volume, L

References

[1] Q. Yu, Y. Yuan, J. Wen, X. Zhao, S. Zhao, D. Wang, C. Li, X. Wang, N. Wang, A universally applicable strategy for construction of anti-biofouling adsorbents for enhanced uranium recovery from seawater, Adv. Sci., 6 (2019) 1900002, doi: 10.1002/advs.201900002.

[2] H. Guo, P. Mei, J. Xiao, X. Huang, A. Ishag, Y. Sun, Carbon materials for extraction of uranium from seawater, Chemosphere, 278 (2021) 130411, doi: 10.1016/j.chemosphere.2021.130411.

[3] H. Zhao, X. Liu, M. Yu, Z. Wang, B. Zhang, H. Ma, M. Wang, J. Li, A study on the degree of amidoximation of polyacrylonitrile fibers and its effect on their capacity to adsorb uranyl ions, Ind. Eng. Chem. Res., 54 (2015) 3101–3106.

[4] J. Zhang, X. Yin, Z. Ye, L. Chen, L. Liu, X. Wang, Y. Zhu, T. Fujita, Y. Wei, Synthesis of novel hierarchical rod-like Mg-Al bimetallic oxides for enhanced removal of uranium(VI) from wastewater, Chemosphere, 308 (2022) 136546, doi: 10.1016/j.chemosphere.2022.136546.

[5] L. Yang, J. Jin, Y.C. Wang, W.Q. An, Y.A. Zhao, C. Cui, L.F. Han, X.K. Wang, The removal of uranium(VI) from aqueous solution by the anaerobically digested sewage sludge with hydrothermal pretreatment, Chemosphere, 288 (2022) 132644, doi: 10.1016/j.chemosphere.2021.132644.

[6] F.Q. Ma, Y.Y. Gui, P. Liu, Y. Xue, W. Song, Functional fibrous materials-based adsorbents for uranium adsorption and environmental remediation, Chem. Eng. J., 390 (2020) 124597, doi: 10.1016/j.cej.2020.124597.

[7] F. Ma, B. Dong, Y. Gui, M. Cao, L. Han, C. Jiao, H. Lv, J. Hou, Y. Xue, Adsorption of low-concentration uranyl ion by amidoxime polyacrylonitrile fibers, Ind. Eng. Chem. Res., 57 (2018) 17384–17393.

[8] L. Yin, B.W. Hu, L. Zhuang, D. Fu, J.X. Li, T. Hayat, A. Alsaedi, X.K. Wang, Synthesis of flexible cross-linked cryptomelane-type manganese oxide nanowire membranes and their application for U(VI) and Eu(III) elimination from solutions, Chem. Eng. J., 381 (2020) 122744, doi: 10.1016/j.cej.2019.122744.

[9] Y. Xie, C.L. Chen, X.M. Ren, X.X. Wang, H.Y. Wang, X.K. Wang, Emerging natural and tailored materials for uranium-contaminated water treatment and environmental remediation, Prog. Mater Sci., 103 (2019) 180–234.

[10] F.L. Liu, S. Hua, C. Wang, B.W. Hu, Insight into the performance and mechanism of persimmon tannin functionalized waste paper for U(VI) and Cr(VI) removal, Chemosphere, 287 (2022) 132199, doi: 10.1016/j.chemosphere.2021.132199.

[11] N. Li, L. Yang, X. Ji, J. Ren, B. Gao, W. Deng, Z. Wang, Bioinspired succinyl-β-cyclodextrin membranes for enhanced uranium extraction and reclamation, Environ. Sci.: Nano, 7 (2020) 3124–3135.

[12] Y. Lee, Y.M. Ren, M.C. Cui, J.J. Ma, Z.C. Han, O. Kwon, J. Ko, J. Khim, Rare earth real wastewater treatment by pilot scale using new concept continuous treatment process, Chemosphere, 279 (2021) 130523, doi: 10.1016/j.chemosphere.2021.130523.

[13] Y. Huang, M. Su, D. Chen, L. Zhu, Y. Pang, Y. Chen, Highly-efficient and easy separation of hexahedral sodium dodecyl sulfonate/δ-FeOOH colloidal particles for enhanced removal of aqueous thallium and uranium ions: synergistic effect and mechanism study, J. Hazard. Mater., 402 (2021) 123800, doi: 10.1016/j.jhazmat.2020.123800.

[14] Z. Lv, H. Wang, C. Chen, S. Yang, L. Chen, A. Alsaedi, T. Hayat, Enhanced removal of uranium(VI) from aqueous solution by a novel Mg-MOF-74-derived porous MgO/carbon adsorbent, J. Colloid Interface Sci., 537 (2019) A1–A10.

[15] J. Xue, H. Zhang, D.X. Ding, N. Hu, Y.-D. Wang, Y.-S. Wang, Linear β-cyclodextrin polymer functionalized multiwalled carbon nanotubes as nanoadsorbent for highly effective removal of U(VI) from aqueous solution based on inner-sphere surface complexation, Ind. Eng. Chem. Res., 58 (2019) 4074–4083.

[16] N. Li, L. Yang, D. Wang, C. Tang, W. Deng, Z. Wang, High-capacity amidoxime-functionalized β-cyclodextrin/graphene aerogel for selective uranium capture, Environ. Sci. Technol., 55 (2021) 9181–9188.

[17] P.H. Ju, K.T. Alali, G.H. Sun, H.S. Zhang, Q. Liu, J.Y. Liu, J. Yu, R.R. Chen, J. Wang, Swollen-layer constructed with polyamine on the surface of nano-polyacrylonitrile cloth used for extract uranium from seawater, Chemosphere, 271 (2021) 129548, doi: 10.1016/j.chemosphere.2021.129548.

[18] S. Yang, J. Yin, Q. Li, C.Y. Wang, D.B. Hua, N. Wu, Covalent organic frameworks functionalized electrodes for simultaneous removal of UO_2^{2+} and ReO_4^- with fast kinetics and high capacities by electro-adsorption, J. Hazard. Mater., 429 (2022) 128315, doi: 10.1016/j.jhazmat.2022.128315.

[19] F. Chi, X. Wang, J. Xiong, S. Hu, Polyvinyl alcohol fibers with functional phosphonic acid group: synthesis and adsorption of uranyl(VI) ions in aqueous solutions, J. Radioanal. Nucl. Chem., 296 (2012) 1331–1340.

[20] H.J. Ma, S.D. Yao, J.Y. Li, C.Q. Cao, M. Wang, A mild method of amine-type adsorbents syntheses with emulsion graft polymerization of glycidyl methacrylate on polyethylene non-woven fabric by pre-irradiation, Radiat. Phys. Chem., 81 (2012) 1393–1397.

[21] M. Ahmad, J. Chen, K. Yang, T. Shah, M.-u.-d. Naik, Q. Zhang, B. Zhang, Preparation of amidoxime modified porous organic polymer flowers for selective uranium recovery from seawater, Chem. Eng. J., 418 (2021) 129370, doi: 10.1016/j.cej.2021.129370.

[22] R.R. Liu, S.X. Wen, Y. Sun, B.J. Yan, J.W. Wang, L. Chen, S.Y. Peng, C. Ma, X.Y. Cao, C.X. Ma, G.G. Duan, S. Shi, Y.H. Yuan, N. Wang, A nanoclay enhanced amidoxime-functionalized double-network hydrogel for fast and massive uranium recovery from seawater, Chem. Eng. J., 422 (2021) 130060, doi: 10.1016/j.cej.2021.130060.

[23] C.M. Thakar, S.S. Parkhe, A. Jain, K. Phasinam, G. Murugesan, R.J.M. Ventayen, 3D printing: basic principles and applications, Mater. Today Proc., 51 (2022) 842–849.

[24] H. Li, K.H. Hu, Y.S. Liu, Z.G. Lu, J.J. Liang, Improved mechanical properties of silica ceramic cores prepared by 3D printing and sintering processes, Scripta Mater., 194 (2021) 113665, doi: 10.1016/j.scriptamat.2020.113665.

[25] F.X. Song, N. Wang, Q.Q. Zhang, W.B. Jie , B. Liu, 3D printing calcium alginate adsorbents for highly efficient recovery of U(VI) in acidic conditions, J. Hazard. Mater., 440 (2022) 129774, doi: 10.1016/j.jhazmat.2022.129774.

[26] Y. Meng, Y. Wang, L. Liu, Y. Fang, F. Ma, C. Zhang, H. Dong, Efficient and magnetically recoverable U(VI) adsorbent: Fe_3O_4 loaded hypercrosslink copoly (styrene/maleic anhydride), Colloids Surf., A, 632 (2022) 127644, doi: 10.1016/j.colsurfa.2021.127644.

[27] K.G. Wei, Q.L. Wang, C.P. Huang, The distribution of adsorption energy of U(VI) onto AEPTES-functionalized porous silica with multiple average pore sizes, Chem. Eng. J., 451 (2023) 138716, doi: 10.1016/j.cej.2022.138716.

[28] L. Ma, H. Ye, L. Liu, M.-B. Wu, J. Yao, Polypropylene membranes with high adsorption capacity and anti-adhesion properties achieved by hydrophobic interactions and hydrogen bonded self-assembly for uranium extraction from seawater, Chem. Eng. J., 451 (2023) 138696, doi: 10.1016/j.cej.2022.138696.

[29] X. Liu, X. Wang, W. Jiang, C.-R. Zhang, L. Zhang, R.-P. Liang, J.-D. Qiu, Covalent organic framework modified carbon nanotubes for removal of uranium(VI) from mining wastewater, Chem. Eng. J., 450 (2022) 138062, doi: 10.1016/j.cej.2022.138062.

[30] J. Yu, C.H. Yu, W.K. Zhu, G.Q. He, Y.X. Wei, J. Zhou, Hydrous titanium oxide and bayberry tannin co-immobilized nano collagen fibrils for uranium extraction from seawater and recovery from nuclear wastewater, Chemosphere, 286 (2022) 131626, doi: 10.1016/j.chemosphere.2021.131626.

[31] Y. Xu, J. Yu, J. Zhu, Q. Liu, H. Zhang, J. Liu, R. Chen, Y. Li, J. Wang, Cyclized polyacrylonitrile amidoxime with local conjugate domain for high-efficiency extraction of uranium from seawater, Appl. Catal., B, 316 (2022) 121677, doi: 10.1016/j.apcatb.2022.121677.

[32] C.J. Li, X.F. Zhang, C.X. Bao, J.M. Zhang, Y.R. Tian, J. Shen, X.Y. Feng, Freezing-induced chemical crosslinking to fabricate nanocellulose-based cryogels for efficient bilirubin

removal, Sep. Purif. Technol., 300 (2022) 121865, doi: 10.1016/j.seppur.2022.121865.
[33] P. Amesh, K.A. Venkatesan, A.S. Suneesh, D.K. Gupta, T.R. Ravindran, Diethylenetriamine functionalized silica gel for adsorption of uranium from aqueous solution and seawater, J. Radioanal. Nucl. Chem., 329 (2021) 337–349.
[34] F. Zhang, Y. Liu, K.Q. Ma, H. Yan, Y. Luo, F.C. Wu, C.T. Yang, S. Hu, S.M. Peng, Highly selective extraction of uranium from wastewater using amine-bridged diacetamide-functionalized silica, J. Hazard. Mater., 435 (2022) 129022, doi: 10.1016/j.jhazmat.2022.129022.
[35] W.J. Liu, Q.L. Wang, H.Q. Wang, Q. Xin, W. Hou, E.M. Hu, Z.W. Lei, Adsorption of uranium by chitosan/chlorella pyrenoidosa composite adsorbent bearing phosphate ligand, Chemosphere, 287 (2022) 132193, doi: 10.1016/j.chemosphere.2021.132193.
[36] X. Xu, H.J. Zhang, J.X. Ao, L. Xu, X.Y. Liu, X.J. Guo, J.Y. Li, L. Zhang, Q.N. Li, X.Y. Zhao, B.J. Ye, D.L. Wang, F. Shen, H.J. Ma, 3D hierarchical porous amidoxime fibers speed up uranium extraction from seawater, Energy Environ. Sci., 12 (2019) 1979–1988.
[37] Y. Wang, Z.W. Lin, J.H. Zhu, J.Y. Liu, J. Yu, Q. Liu, R.R. Chen, Y. Li, J. Wang, Co-construction of molecular-level uranyl-specific "nano-holes" with amidoxime and amino groups on natural bamboo strips for specifically capturing uranium from seawater, J. Hazard. Mater., 437 (2022) 129407, doi: 10.1016/j.jhazmat.2022.129407.
[38] Z. Chen, X. He, Q. Li, H. Yang, Y. Liu, L. Wu, Z. Liu, B. Hu, X. Wang, Low-temperature plasma induced phosphate groups onto coffee residue-derived porous carbon for efficient U(VI) extraction, J. Environ. Sci., 122 (2022) 1–13.
[39] R. Liu, H. Wang, L. Han, B. Hu, M. Qiu, Reductive and adsorptive elimination of U(VI) ions in aqueous solution by SFeS@biochar composites, Environ. Sci. Pollut. Res., 28 (2021) 55176–55185.
[40] N. Li, P. Gao, H.W. Chen, F.L. Li, Z.N. Wang, Amidoxime modified Fe_3O_4@TiO_2 particles for antibacterial and efficient uranium extraction from seawater, Chemosphere, 287 (2022) 132137, doi: 10.1016/j.chemosphere.2021.132137.
[41] S. Shi, R. Wu, S.L. Meng, G.P. Xiao, C.X. Ma, G.C. Yang, N. Wang, High-strength and anti-biofouling nanofiber membranes for enhanced uranium recovery from seawater and wastewater, J. Hazard. Mater., 436 (2022) 128983, doi: 10.1016/j.jhazmat.2022.128983.
[42] N. Tang, J. Liang, C. Niu, H. Wang, Y. Luo, W. Xing, S. Ye, C. Liang, H. Guo, J. Guo, Y. Zhang, G. Zeng, Amidoxime-based materials for uranium recovery and removal, J. Mater. Chem. A, 8 (2020) 7588–7625.

Supporting information

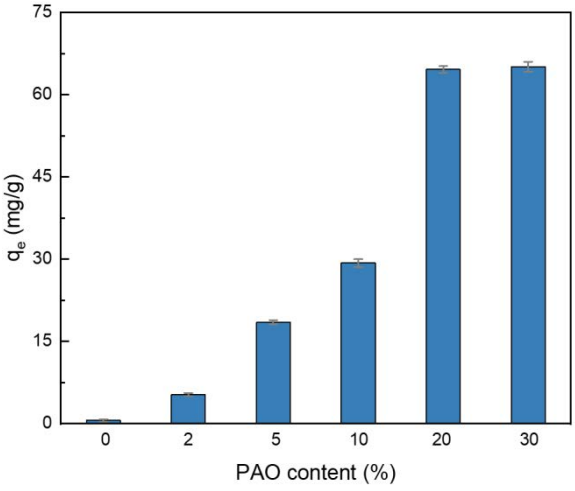

Fig. S1. Effect of poly(amidoxime) content on uranium adsorption capacity.

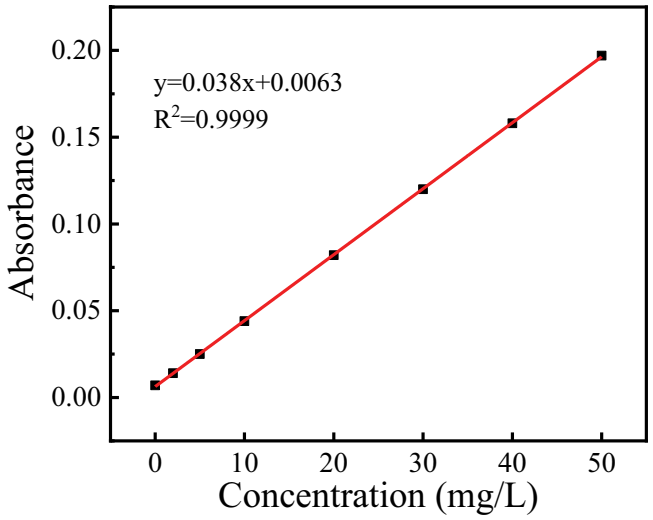

Fig. S2. Uranium standard curve.

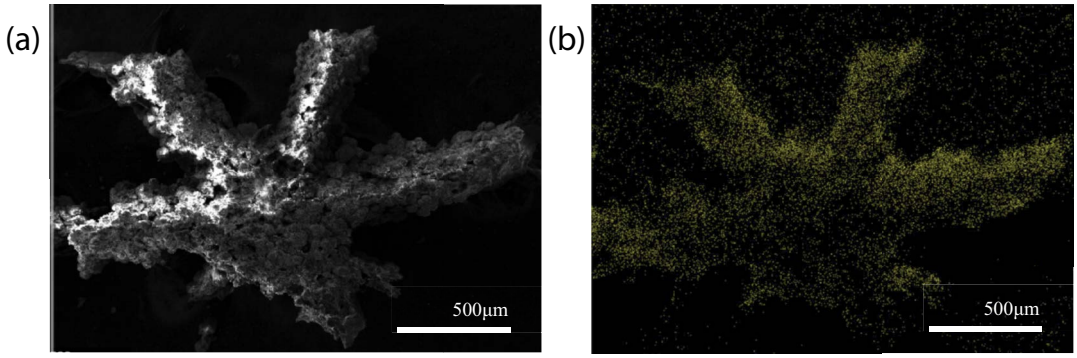

Fig. S3. (a) Scanning electron microscopy image and U of 3D-PAO/U and (b) distribution of U on 3D-PAO/U.

Table S1
Zeta potential of PAN and poly(amidoxime)

Materials	Zeta potential (mV)	Mob (μmcm/Vs)
PAN	–12.96	–1.015
Poly(amidoxime)	–2.902	–0.2277

Table S2
Adsorption isotherm parameters obtained from the Langmuir, Freundlich and Temkin models in the adsorption of U(VI) onto 3D-PAO

Models	Parameters	
Langmuir	q_{max}	78.01
	K_L	3.05×10^{-2}
	R^2	0.9863
Freundlich	$1/n$	0.9477
	K_f	3.21
	R^2	0.9692
Temkin	a	42.84
	b	–5.89
	R^2	0.8512

Table S4
Content of C, N, O and U elements on 3D-PAO/U

Elements	Mass ratio (%)	Atomic (%)
C	33.56	42.23
N	17.69	19.09
O	39.20	37.03
U	7.03	0.45

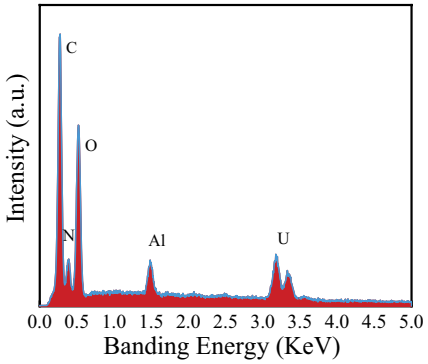

Fig. S4. Local element analysis of 3D-PAO/U.

Table S3
Comparison of 3D-PAO and reported studies on adsorbents for U(VI) adsorption

Adsorbents	Adsorption capacity (mg/g)	Tunable macroscopic structure	References
Wool-g-AO	59.35	NO	[S1]
MC-CA	13.00	NO	[S2]
AO-MWCNTs	67.90	NO	[S3]
PAO/MoS_2	47.40	NO	[S4]
PA66-g-PGMA-IDPAO	41.98	NO	[S5]
AO-OBHSPIM	244.0	NO	[S6]
AO-resin	79.87	NO	[S7]
3D-PAO	78.01	Yes	This work

References

[S1] Z. Yin, J. Xiong, M. Chen, S. Hu, H. Cheng, Recovery of uranium(VI) from aqueous solution by amidoxime functionalized wool fibers, J. Radioanal. Nucl. Chem., 307 (2015) 1471–1479.
[S2] M. Carboni, C.W. Abney, K.M.L. Taylor-Pashow, J.L. Vivero-Escoto, W. Lin, Uranium sorption with functionalized mesoporous carbon materials, Ind. Eng. Chem. Res., 52 (2013) 15187–15197.
[S3] J. Wu, K. Tian, J. Wang, Adsorption of uranium(VI) by amidoxime modified multiwalled carbon nanotubes, Prog. Nucl. Energy, 106 (2018) 79–86.
[S4] D. Shao, X. Liu, T. Hayat, J. Li, X. Ren, Poly(amidoxime) functionalized MoS_2 for efficient adsorption of uranium(VI) in aqueous solutions, J. Radioanal. Nucl. Chem., 319 (2018) 379–386.
[S5] M. Zhang, Q. Gao, C. Yang, L. Pang, H. Wang, H. Li, R. Li, L. Xu, Z. Xing, J. Hu, G. Wu, Preparation of amidoxime-based nylon-66 fibers for removing uranium from low-concentration aqueous solutions and simulated nuclear industry effluents, Ind. Eng. Chem. Res., 55 (2016) 10523–10532.
[S6] L. Zhu, C. Zhang, F. Ma, C. Bi, R. Zhu, C. Wang, Y. Wang, L. Liu, H. Dong, Hierarchical self-assembled polyimide microspheres functionalized with amidoxime groups for uranium-containing wastewater remediation, ACS Appl. Mater. Interfaces, 15 (2023) 5577–5589.
[S7] F. Lei, W.B. Zhang, Y. Zhou, N.Y. Zhou, T.H. Liu, K.L. Shi, W.S. Wu, X.Q. Gao, J.Q. Yang, Efficient removal of uranium from wastewater using amidoxime-carboxyl functional resin with large particle size, J. Radioanal. Nucl. Chem., (2022), doi: 10.1007/s10967-022-08711-5.